Study of incoherent x-radiation induced by relativistic electrons in crystals

V. B. Gavrikov,[1] V. P. Likhachev,[2] J. D. T. Arruda-Neto,[2,3] and A. L. Bonini[2]
[1]*Kharkov Institute of Physics and Technology, 1 Akademishna 61108 Kharkov, Ukraine*
[2]*Laboratório do Acelerador Linear, Instituto de Física da Universidade de São Paulo, CP66318, 05315-970 São Paulo, SP, Brazil*
[3]*University of Santo Amaro/UNISA, Rua Prof. Eneas de Sequeira Neto, 340, 04829-300 São Paulo, SP, Brazil*
(Received 15 August 2001; published 15 January 2002)

Features of incoherent x-ray radiation, produced by relativistic electrons with energy of several tens of MeV in crystals, are studied for observation angles exceeding γ^{-1} (γ is the projectile Lorentz factor) and for all possible momentum transfer. It is shown that the fivefold cross section has a pronounced structure, with sharp maxima and a minimum. A Monte Carlo procedure is developed to obtain a threefold cross section and, then, contributions of different radiation mechanisms are analyzed. The results of numerical integration are compared with experimental ones, and a good agreement between them is verified. The obtained results can be used both in experimental investigations dealing with interaction of charged particle beams with crystals, and to optimize parameters of x-ray sources based on the coherent x-radiation process.

DOI: 10.1103/PhysRevA.65.022903 PACS number(s): 79.20.Kz, 41.75.Ht, 78.70.Ck

I. INTRODUCTION

In the course of the last decade the properties of coherent x radiation, which is produced by a relativistic charged particle in a crystalline target, have been widely studied both theoretically and experimentally. In particular, great efforts were directed to investigate the radiation induced by electron beams with energies of several tens of MeV. At these beam energies the absolute intensity [1,2], spectral-angular dependencies [2–4], and interference effect [5–6] were investigated. A possibility to design quasimonochromatic, tunable and polarized x-radiation sources using moderate electron-beam energies on the base of the process was discussed in [4].

At the same time, incoherent bremsstrahlung accompanying the passage of a relativistic particle through a crystalline target was studied but only in earlier works [7,8]. In these works the reaction of crystal electrons was not considered, and it was restricted only to the case where projectiles radiate in screened fields of crystal nuclei in near-forward directions.

The goal of the present paper is the theoretical and experimental study of the incoherent x radiation, produced by electrons with several tens MeV of energy in crystalline target at observation angles $\theta_\gamma > \gamma^{-1}$ (where γ is the projectile Lorentz factor), i.e., for those observation angles where the contribution of crystal electrons to the total radiation yield is comparable with the static situation, or dominates in the whole process for all possible momentum transfer. Our main task is to investigate properties of the differential cross section with respect to the outgoing electron solid angle and the energy, and the solid angle of bremsstrahlung photon (fivefold), as well as the differential cross section with respect to the photon solid angle and energy (threefold). To our knowledge, there are no expressions which would allow one to make exact calculations of these cross sections in the full momentum transfer region, and by taking all radiation channels into account. For this reason, we subdivide the momentum range into two regions and carry out calculations by making suitable approximations for each region.

The obtained results allow us to carry out the analysis of experiments using finite-size detectors as well as to define those conditions for coincidence experiments where the incoherent x-ray yield is minimal. The results for incoherent cross section integrated over the angles of the final electron permit us to find an exact ratio between the coherent and incoherent components of the radiation, which is important from the point of view of a practical utilization of the coherent x-radiation process.

II. RADIATION CROSS SECTION

We consider a relativistic electron with initial energy E_1, momentum $\vec{p}_1$, and velocity $\vec{v}_1$, which interacts with a crystalline target, and as a result, in the final state there are the electron with final energy E_2, momentum $\vec{p}_2$, velocity $\vec{v}_2$, and a bremsstrahlung photon with wave vector $\vec{k}$ and energy ω, which is emitted into a solid angle $d\Omega_\gamma$ around an observation angle θ_γ. During the radiation the medium acquires the momentum $\vec{q}=\vec{p}_1-\vec{p}_2-\vec{k}$.

In our paper we span the possible momentum transfer into two regions. The first corresponds to those momentum where the projectile interacts with a crystal atom as a whole and, therefore, the long-wavelength approximation is valid. As a result, the interference effect between different radiation mechanisms is essential. In the second region, a region of large momentum transfer, each atomic component acts as an individual particle.

On the assumption that the inequalities $\omega \ll E_1, \omega \ll E_2$ are satisfied for all relevant photon energies and, moreover, the radiation energies are large compared to the electronic binding energies, the radiation cross section per atom in the crystal can be expressed by means of a radiation cross section for an isolated atom, $d\sigma_{at}$, and a diffraction factor, as done in the theory of high-energy coherent bremsstrahlung [8,9]:

$$d\sigma_{\rm cr}=(f_{\rm inc}+f_{\rm coh})d\sigma_{\rm at}=d\sigma_{\rm inc}+d\sigma_{\rm coh}, \qquad (1)$$

where the coherent, $f_{\rm coh}$, and incoherent, $f_{\rm inc}$, parts of the diffraction factor are

 ©2002 The American Physical Society

$$f_{\mathrm{inc}}=1-\exp(-q^2u^2),$$

$$f_{\mathrm{coh}}=\frac{(2\pi)^3}{V_cN}\exp(-q^2u^2)\sum_{\vec{g}} D^2(\vec{q})\,\delta(\vec{q}-\vec{g})$$

and u^2 is the mean-square temperature displacement of the atoms from their equilibrium positions, V_c is the volume of the unit crystal cell, $\vec{g}$ is a reciprocal lattice vector, N is the number of atoms per unit cell, and $D(\vec{q})$ is the crystal structure factor.

It is seen from Eq. (1) that the coherent cross section, $d\sigma_{\mathrm{coh}}$, differs from zero only if a momentum transfer to the crystal is equal to one of $\vec{g}$. In contrast to $d\sigma_{\mathrm{coh}}$, a momentum transfer spectrum for the incoherent process allows continuum.

We will now consider approximations to calculate the atomic cross section, which are suitable for all possible momentum transfer in the considered photon energy range.

It is well known that there are two mechanisms leading to the appearance of bremsstrahlung at the interaction of the projectile with an atom. The first is due to the interaction of the projectile with the Coulomb field of the nuclear charge; it is the so-called static (Bethe-Heitler) bremsstrahlung. The amplitude of this radiation in the case of unscreened nucleus is well known [10], and for our purposes it can be presented in the form ($\hbar=c=1$):

$$M_{\mathrm{st}}=\frac{(2\pi)^{3/2}e^3}{m(E_1E_2\omega)^{1/2}}\frac{Z}{\gamma q^2}\vec{e}_f\left[\frac{\vec{p}_1}{\omega-\vec{k}\vec{v}_1}-\frac{\vec{p}_2}{\omega-\vec{k}\vec{v}_2}\right], \qquad (2)$$

where $\vec{e}_f$ is the polarization vector of the photon, e and m are the electron charge and mass, respectively, and Z is the atomic number of the crystal.

The second radiation mechanism is connected with the dynamic polarization of the atomic electrons in the field of the incoming particle, and with the bremsstrahlung photon. The general expression for the polarization amplitude, in the case of a nonrelativistic atom, has been obtained by Amus 'ya *et al.* [11] and it is presented in the form [12]

$$M_{\mathrm{pol}}=\frac{(2\pi)^{3/2}e}{(E_1E_2\omega)^{1/2}}\vec{e}_f\,\frac{\omega\vec{v}_1-\vec{q}}{(\vec{k}+\vec{q})-k^2}\,\omega\alpha(\omega,q), \qquad (3)$$

where $\alpha(\omega,q)$ is the dynamic polarizability of the atom. Note that the process described by M_{pol} is equivalent to the coherent Rayleigh scattering of virtual photons associated with the projectile.

A. Small-q region

In this region the projectile interacts with the atom as a whole. The radiation amplitude is a sum of M_{st} and M_{pol}. For the photon energies under consideration, the function $\alpha(\omega,q)$ in Eq. (3) can be replaced by $-e^2F(q)/m\omega^2$, where $F(q)$ is the form factor of the atom. The total radiation cross section, summed over photon polarizations, has the form [12]

$$d\sigma_{\mathrm{at}}=d\sigma_{\mathrm{st}}+d\sigma_{\mathrm{pol}}+d\sigma_{\mathrm{int}}, \qquad (4)$$

where $d\sigma\equiv d^5\sigma/d\omega d\Omega_\gamma d\Omega_{p_2}$ and

$$d\sigma_{\mathrm{st}}=\sigma_0(\omega)Z^2p_2^2\left[\frac{[1-F(q)](\vec{n}\times\vec{q})}{\gamma q^2(1-\beta\cos\theta_\gamma)}\right]^2,$$

$$d\sigma_{\mathrm{pol}}=\sigma_0(\omega)Z^2p_2^2\left[F(q)\,\frac{\vec{n}\times(k\vec{\beta}-\vec{q})}{(\vec{k}+\vec{q})^2-k^2}\right]^2,$$

$$d\sigma_{\mathrm{int}}=\sigma_0(\omega)Z^2p_2^2\left[\frac{[1-F(q)](\vec{n}\times\vec{q})}{\gamma q^2(1-\beta\cos\theta_\gamma)}\right]\times\left[F(q)\,\frac{\vec{n}\times(k\vec{\beta}-\vec{q})}{(\vec{k}+\vec{q})^2-k^2}\right].$$

In Eq. (4) $\sigma_0(\omega)=\alpha r_e^2/\pi^2\omega$, $\alpha=1/137$, r_e is the classical electron radius, $\vec{\beta}\equiv\vec{v}_1$, $\vec{n}=\vec{k}/k$, and $d\Omega_{p2}$ is a solid angle around the direction of $\vec{p}_2$. $d\sigma_{\mathrm{st}}$ and $d\sigma_{\mathrm{pol}}$ represent the static and polarization contributions, respectively, and $d\sigma_{\mathrm{int}}$ describes the contribution resulting from the interference effect between these processes.

B. Atomic electron contribution

Another channel making contributions to the resulting radiation yield in the small-q region, is the radiation of the atomic electrons in collision with the projectile. In this case, each atomic electron acts as an individual particle. This process is equivalent to the Compton scattering of virtual photons associated with the projectile by the bound electrons. In our photon energy region the condition $\omega\ll m$ is fulfilled always. At high electron energy the corresponding cross section, $d\sigma_{\mathrm{el}}$, can be calculated using the equivalent-photon approximation. This cross section can be presented as the product of three terms: the elastic (Thomson) scattering cross section, $d\sigma_T$, the number of equivalent photons $n(\omega,\vec{k}_\perp)$ in the spectrum of the projectile field, and $ZS(q)$, where $S(q)$ is the incoherent-scattering function, which is measure of electron binding ([13]):

$$d\sigma_{\mathrm{el}}=Zd\sigma_Tn(\omega,\vec{k}_{1\perp})S(q),n(\omega,\vec{k}_{1\perp})=\frac{\alpha}{\pi^2\omega}\,\frac{k_{1\perp}^2}{(k_{1\perp}^2+\gamma^{-2}\omega^2)^2}\,d\vec{k}_{1\perp}d\omega. \qquad (5)$$

The function $n(\omega,\vec{k}_{1\perp})$ in Eq. (5) defines the number of equivalent photons with energy ω, which are perpendicular with respect to the projectile velocity component, $\vec{k}_{1\perp}$, of the wave vector $\vec{k}_1$; the longitudinal component satisfies the equality $\vec{k}_{1\|}\vec{\beta}=\omega$. The connection between the wave vectors of equivalent and real photons is $\vec{k}_1=\vec{k}+\vec{q}$, and for a fixed photon energy $d\vec{k}_1=d\vec{k}_{1\perp}=d\vec{q}$.

The Thomson cross section is

$$d\sigma_T=r_e^2\sin^2\theta' d\Omega_\gamma, \qquad (6)$$

where θ' is the angle between the initial photon polarization vector and the observation direction. The polarization direction of equivalent photons coincides with $\vec{k}_{1\perp}$ and, therefore,

$$\sin\theta' = \frac{1}{k_{1\perp}}(\vec{n}\times\vec{k}_{1\perp}). \tag{7}$$

Replacing $d\vec{q}$ by $p_2^2 d\Omega_{p_2}$, $k_{1\perp}^2$ by $k_1^2 - k_{1\|}^2 = (\vec{k}+\vec{q})^2 - \beta^{-2}k^2$, and taking into account that $\gamma \gg 1$ plus Eqs. (6) and (7), we can finally write

$$d\sigma_{\rm el} = \sigma_0(\omega) Z p_2^2 \left[\frac{\vec{n}\times(k\vec{\beta}-\vec{q})}{(\vec{k}+\vec{q})^2 - k^2}\right]^2 S(q). \tag{8}$$

Since $S(q)$ is defined in the whole momentum transfer region, $d\sigma_{\rm el}$ contributes to the total radiation cross section both in the small and large-q regions.

C. Large-q region

This region corresponds to those momentum transfers where each atomic electron interacts with the projectile independently, and the projectile radiates in the fields of the nucleus and each of the atomic electrons. Using Eq. (2) the cross section of projectile radiation can be written in the form

$$d\sigma_{\rm nc} = \sigma_0(\omega)\frac{Z(Z+1)}{\gamma^2 q^4} p_2^2 \left[\frac{\vec{n}\times\vec{p}_1}{1-v_1\cos\theta_\gamma} - \frac{\vec{n}\times\vec{p}_2}{1-v_2\cos\theta_2}\right]^2, \tag{9}$$

where the angle θ_2 describes the final projectile motion direction with respect to $\vec{k}$. In Eq. (9) we take into account that the projectile radiates in the Coulomb field of atomic electrons as in the nuclear field with $Z=1$ [14]. Additional contribution to the cross section in this region arises from $d\sigma_{\rm el}$, Eq. (8).

III. INTEGRATION PROCEDURE

To integrate $d\sigma_{\rm inc}$ over the outgoing electron angles we define the boundary between the small and large momentum transfer regions as $q_b = 5a^{-1}$, where $a = 0.885 a_0 Z^{-1/3}$ is a screening (Thomas-Fermi) radius with a_0 the Bohr radius. Using notation $d^3\sigma \equiv d^3\sigma/d\omega d\Omega_\gamma$, the threefold spectral-angular incoherent cross section is then defined as

$$d^3\sigma_{\rm inc} = \int_{q_{\rm min}\leqslant q\leqslant q_b} f_{\rm inc}(d\sigma_{\rm at} + d\sigma_{\rm el}) d\Omega_{p2} + \int_{q_b\leqslant q\leqslant q_{\rm max}} f_{\rm inc}(d\sigma_{\rm el} + d\sigma_{\rm nc}) d\Omega_{p2}. \tag{10}$$

Taking the inequalities $k \ll p_1, p_2$ into account, it can be seen from energy and momentum conservation that the q's range is $q_{\rm min}\leqslant q\leqslant q_{\rm max}$, where

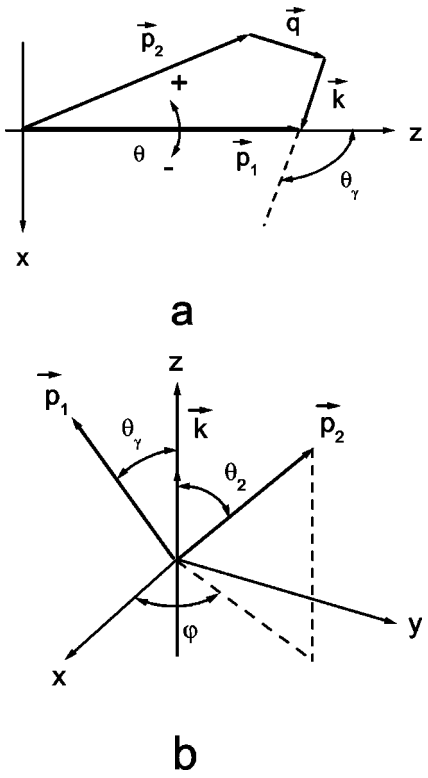

FIG. 1. The coordinate systems and definitions used in the paper: $\vec{k}$ is the photon wave vector of a bremsstrahlung photon; $\vec{p}_1$ and $\vec{p}_2$ are the initial and final projectile momenta, respectively; $\vec{q}$ is the momentum transfer; θ_γ is the observation angle. (a) The laboratory coordinate system. The z axis is directed along $\vec{p}_1$, the vectors $\vec{p}_1$ and $\vec{k}$ lie in the xz plane, θ is the angle between the initial and final motion directions in the case, when $\vec{p}_2$ lies in the xz plane. (b) The photon related coordinate system. The z axis is directed along $\vec{k}$, the vectors $\vec{p}_1$ and $\vec{k}$ lie in the xz plane, θ_2 is the angle between $\vec{p}_2$ and $\vec{k}$, and φ is the angle between the planes $(\vec{k},\vec{p}_1)$ and $(\vec{k},\vec{p}_2)$.

$$q_{\rm min} = k(1-\cos\theta_\gamma) + \frac{1}{2}\frac{k^2}{p_1}(1+\sin^2\theta_\gamma) + O(k^3/p_1^2) \tag{11}$$

and $q_{\rm max} \approx 2p_2$.

To demonstrate peculiarities of $d\sigma_{\rm inc}$ we use the coordinate system where the z axis is directed along $\vec{p}_1$, and the vectors $\vec{p}_1$ and $\vec{k}$ lie in the xz plane [Fig. 1(a)]. The angular dependence of $d\sigma_{\rm inc}$ on θ in the small-q region, where θ is the angle between $\vec{p}_1$ and $\vec{p}_2$ when $\vec{p}_2$ lies in the xz plane, is shown in Fig. 2 for the cases of silicon crystal and noncrystal targets, for photon energies 5 and 20 keV, $E_1 = 15$ MeV, and $\theta_\gamma = 40°$. As it seems from this figure $d\sigma_{\rm inc}$ has a complex character in the small-q region and, therefore, considerable care is required in the numerical integration.

To avoid cancelations and losses of sharp structure effects in the fivefold differential cross section, the integration in Eq. (10) is most conveniently accomplished in the photon-oriented coordinate system [Fig. 1(b)], a spherical coordinate system where the polar axis coincides with the photon momentum direction. In this system, the angles θ_γ and θ_2 de-

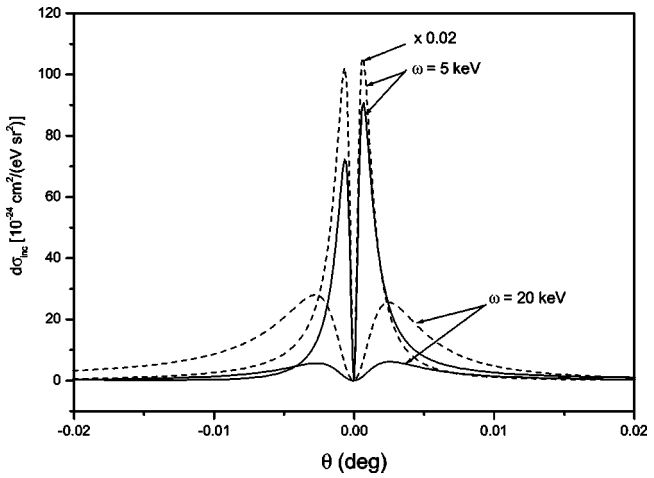

FIG. 2. Dependence of the fivefold incoherent cross section $d\sigma_{inc}$ on θ in the small-q region [see Fig. 1(a)], for $\omega=5$ and 20 keV, $E_1=15$ MeV, and $\theta_\gamma=40°$. Solid and dashed lines correspond to silicon crystal and amorphous targets, respectively.

scribe the initial and final electron momentum directions, and φ is the angle between the $(\vec{k},\vec{p}_1)$ and $(\vec{k},\vec{p}_2)$ planes. At integration, the values of $F(q)$ and $S(q,Z)$ were obtained by linear interpolation from values given in [13].

In the small-q region the angle φ was generated randomly in the range $\pm\varphi_{\max}$ with uniform distribution. The angle θ_2 was generated randomly in the range $[\theta_{\min},\theta_{\max}]$ with the uniform distribution in $\cos\theta_2$:

$$\theta_2=\arccos[\cos\theta_{\min}-(\cos\theta_{\min}-\cos\theta_{\max})\xi],$$

where ξ is a chance number uniformily distributed in the range [0, 1]; $\theta_{\min}$, $\theta_{\max}$, and $\varphi_{\max}$ are the angular limits in the photon-oriented system corresponding to $q=q_b$.

For the large-q region the Monte Carlo procedure generated φ uniformly in the range up to 2π and θ_2 in the range up to π with the same distribution as for the small-q region.

In the small-q region the set of the three generated angles θ_γ, θ_2, and φ was used for the calculation of q, and if q was less than q_b, this set was used to calculate the average fivefold differential cross section:

$$\langle d\sigma\rangle=\frac{1}{N}\sum_{i=1}^{N} d\sigma_i,$$

and then to define the threefold cross section

$$d^3\sigma=\langle d\sigma\rangle\Delta\Omega,$$

where $\Delta\Omega$ is the secondary electron solid angle, which was also calculated by MC simulation in the photon-oriented system [15] where N is the number of the MC starts. For the large-q region the filter was not used and it was supposed that $\Delta\Omega=4\pi$. In our calculations N was 10^7 and 10^8 for the small and large-q regions, respectively.

Note that with the above choice of q_b the integration of $f_{\rm inc}d\sigma_{\rm at}$ in the large-q region gives only a few percent contribution to a final result obtained for the small-q region.

In contrast with the small-q region, in the region of large momentum transfer $d\sigma_{\rm inc}$ changes smoothly, and for this region analytical expressions for the threefold cross sections can be found. By assuming that $q\gg k$ and using the small-angle approximation we found with logarithmic accuracy the following results for the threefold cross sections in the large-q region:

$$d^3\sigma_{\rm nc}=\frac{\pi\sigma_0(\omega)Z(Z+1)}{\gamma^2(1-v_1\cos\theta_\gamma)^2}(1+\cos^2\theta_\gamma)\times\left[\ln\left(\frac{q_{\max}}{q_b}\right)-\frac{1}{2}\mathrm{Ei}(u^2q_{\max}^2,u^2q_b^2)\right] \quad (12)$$

and

$$d^3\sigma_{\rm el}=\pi\sigma_0(\omega)Z(1+\cos^2\theta_\gamma)\times\left[\ln\left(\frac{q_{\max}}{q_b}\right)-\frac{1}{2}\mathrm{Ei}(u^2q_{\max}^2,u^2q_b^2)\right], \quad (13)$$

where we noted $\mathrm{Ei}(x,y)=\int_x^y t^{-1}\exp(-t)dt$. This function appears due to the exponential term in $f_{\rm inc}$; without this function Eqs. (12) and (13) present the cross sections of the radiation for an amorphous target.

IV. RESULTS AND DISCUSSION

A. Numerical results

Figures 3–5 show the results of the MC calculations of different contributions to the incoherent cross section as functions of the observation angle. It is assumed that the incoherent radiation is generated by electrons having energy 15 MeV and passing through a silicon target kept at room temperature.

In Fig. 3(a) the contributions of various radiation mechanisms at the small-q region are presented for photon energy 5 keV and for a crystal target. It is seen from this figure that the total electron contribution, i.e., the polarization and the atomic electron contributions, begins to play an essential role in the total radiation picture only at $\theta_\gamma>20°$. In this case the polarization contribution predominates over the atomic electron one; they both have the maximal values near the backward observation direction. For the same photon energy, Fig. 3(b) shows the contributions to the cross section in the large-q region in comparison with the total electron contribution from the small-q region. The solid lines are the analytical results of Eqs. (12) and (13). In calculating Ei (x,y) the algorithm described in [16] was used. As it follows from Fig. 3(b), at $\theta_\gamma>30°$ the incoherent radiation from the crystal is formed mainly by the atomic electrons.

In Fig. 4 the contributions to the cross section resulting from the small-q region are presented for a photon energy of 20 keV. It is seen that as the photon energy increases the ratio between the polarization contribution and that from the atomic electron changes drastically. As for low photon energies, $d^3\sigma_{el}$ achieves its maximal value near the backward observation direction and dominates at these angles; the

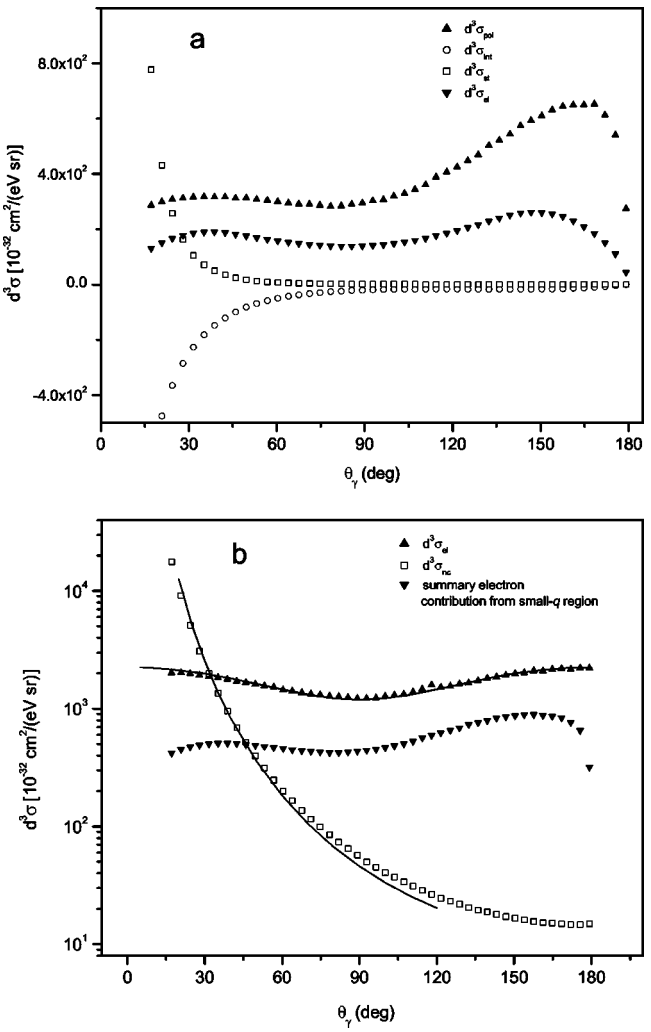

FIG. 3. The threefold incoherent cross section at $\omega=5$ keV and $E_1=15$ MeV in a silicon crystal. (a) The contributions to the incoherent cross section in the small-q region as functions of the observation angle. (b) Comparison between the contributions in the large-q region with the total electron contribution in the small-q region. Solid lines: calculations from Eqs. (12) and (13).

maximum of $d^3\sigma_{\rm pol}$ shifts to the region of small observation angles.

In analogy with Fig. 3(a), Fig. 5(a) shows the contributions of various radiation mechanisms at the small-q region obtained for a silicon amorphous target and for photon energy 5 keV. The contributions to the cross section in the large-q region are compared with the total electron contribution from the small-q region in Fig. 5(b). These figures explicitly show that at $\theta_\gamma > 17°$ the predominant role in the formation of the incoherent radiation from the amorphous target is played by the polarization radiation mechanism.

By using Eqs. (12) and (13) it can be found that the static and atomic electron contributions in the large-q region become equal at observation angles satisfying the equation

$$\cos\theta_\gamma = \frac{1}{v_1}\left(1-\frac{\sqrt{Z+1}}{\gamma}\right). \qquad (14)$$

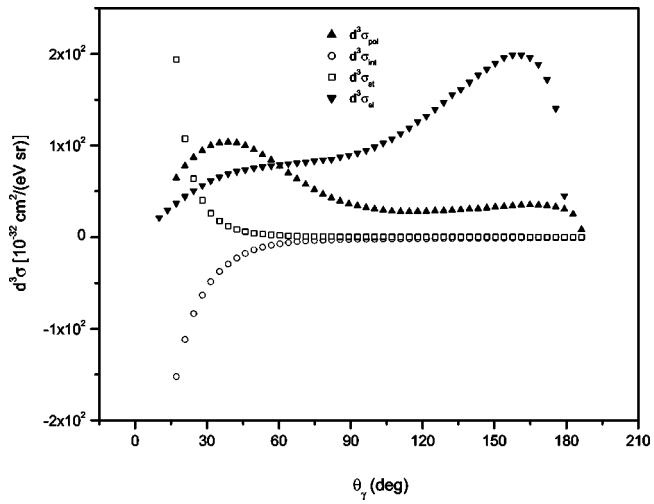

FIG. 4. The contributions to the threefold incoherent cross section in the small-q region as functions of the observation angle at $\omega=20$ keV and $E_1=15$ MeV in a silicon crystal.

Equation (14) gives $\theta_\gamma=29.3°$ for $E_1=15$ MeV and 22.6° for $E_1=25$ MeV. These values are in a good agreement with the Monte Carlo results.

B. Experiment

The experimental investigation of incoherent spectra has been carried out on the Kharkov 40 MeV linear electron accelerator (LUE-40). We have observed the spectra produced in a 30-μm-thick silicon crystal at an electron-beam energy of 15 MeV. The photon detector used was a 5-mm-thick Si(Li) solid-state detector, enclosed by a 25-μm Be window and placed directly into the vacuum photon channel, which is located at an angle of 17.53° with respect to the beam axis. The detector energy resolution was 360 eV and the solid angle, subtended by the detector, was 4.49×10^{-7} sr. Coincidence gating was used and the beam current was adjusted so that the total count rate did not exceed 0.2 counts per beam burst. The average beam current for this condition was 10^{-9} A. A more detailed description of the experimental layout and the procedures is given in [17].

Figure 6 shows a typical measured bremsstrahlung spectrum. In this figure the peak corresponds to the coherent x radiation resulting from the interaction of the projectiles with (111) crystallographic planes. Figure 7 shows the incoherent spectrum obtained by averaging over 9 spectra, which are like the spectrum shown in Fig. 6. Note that the experimental errors ($\pm10\%$) include both statistical errors and the errors resulting from the electron charge measurement procedures. In Fig. 7 the solid line represents the calculation of spectrum, which takes the multiple-scattering and photon attenuation effects into account, the dashed line corresponds to the calculation for an amorphous silicon target having the same thickness as the crystal. The dotted line in Fig. 7 presents the calculation of spectrum for the case of the amorphous target in the large-q region. It is seen from the figure that in this region the difference between the crystal and noncrystal cases does not exceed 10%.

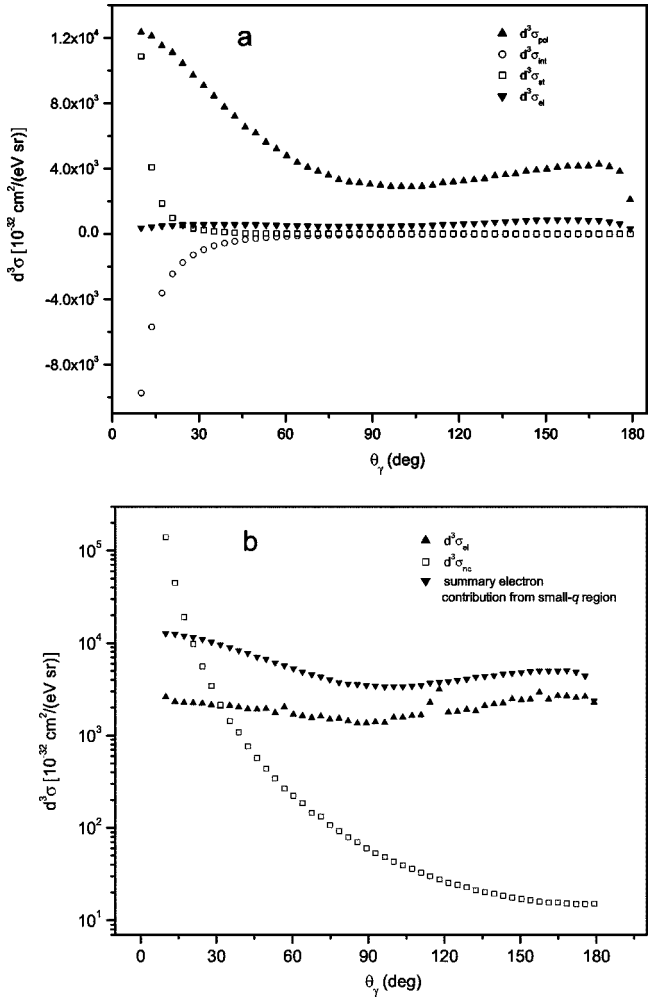

FIG. 5. The threefold incoherent cross section at $\omega=5$ keV and $E_1=15$ MeV in a silicon amorphous target. (a) The contributions to the incoherent cross section in the small-q region as functions of the observation angle. (b) Comparison between the contributions in the large-q region with the total electron contribution in the small-q region.

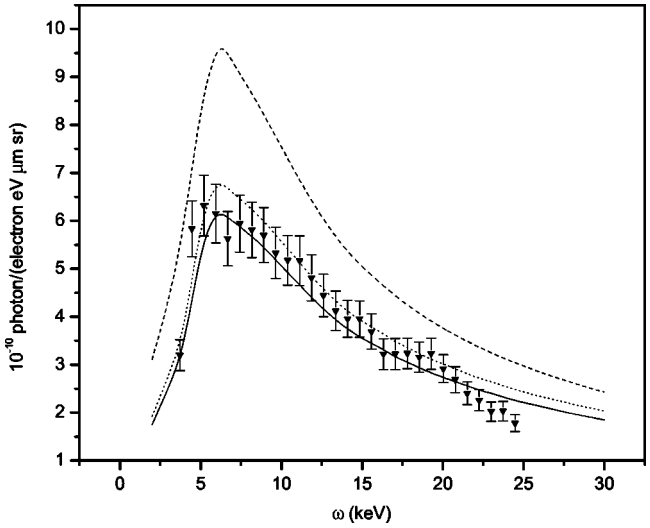

FIG. 7. Dependency of incoherent radiation yield on ω measured in a 30-μm-thick silicon crystal at electron-beam energy of 15 MeV and $\theta_\gamma=17.53°$. Solid line, total threefold cross section taking into account the multiple-scattering and photon attenuation effects in the target; dashed line, calculation for an amorphous silicon target with the same thickness as the crystal; dotted line, calculation for the amorphous case in the large-q region.

As it follows from Eqs. (12) and (13), at fixed θ_γ the static contribution depends on the projectile energy as $\gamma^{-2}\ln\gamma$, and the polarization one as $\ln\gamma$. The multiple-scattering process in a target essentially changes the observed dependencies of radiation yield on the projectile energy in a real experiment, using a finite-size detector. For a crystal of finite thickness L, the radiation yield will be proportional to

$$\frac{\theta_D^2}{\chi_c^2}(d\sigma_{\rm nc}+d\sigma_{\rm el}), \tag{15}$$

where $\chi_c=\chi_c(\gamma,L)$ is the characteristic scattering angle [18] and θ_D is the angular detector size. Because $\chi_c\sim\gamma^{-1}$, in the

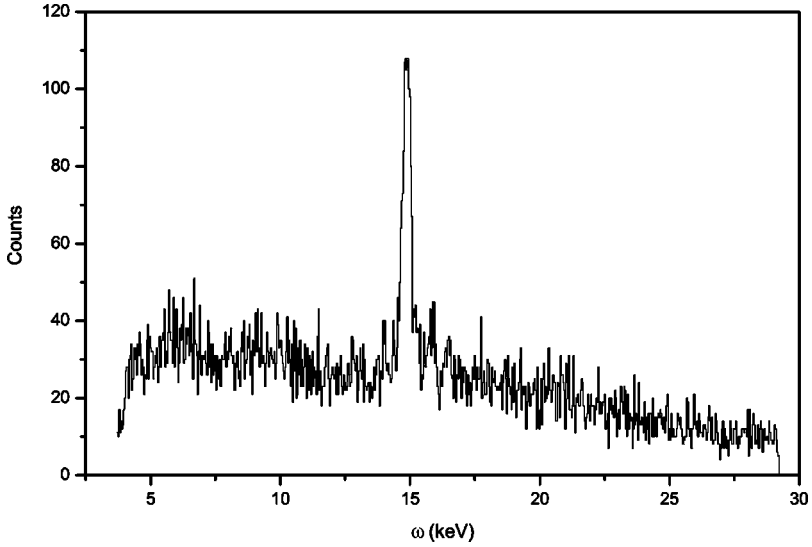

FIG. 6. A typical radiation spectrum measured in a 30-μm-thick silicon crystal at electron beam energy 15 MeV and $\theta_\gamma=17.53°$. The coherent radiation is generated on a set of (111) crystallographic planes.

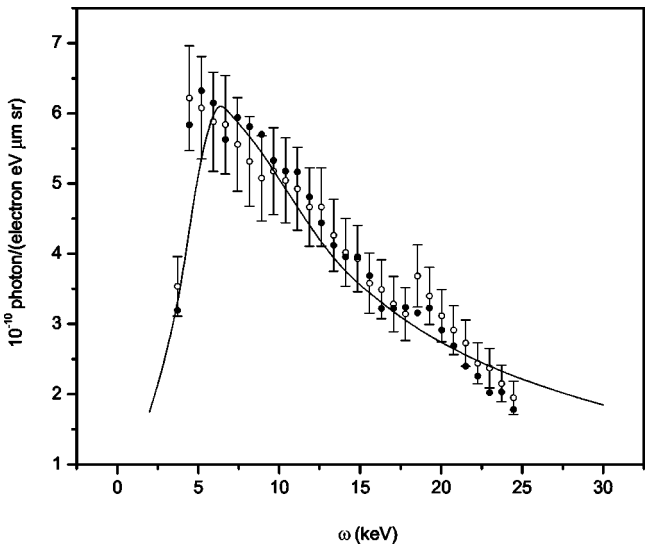

FIG. 8. Comparison between dependencies of incoherent radiation yields on ω measured in a 30-μm-thick silicon crystal at electron-beam energy 15 MeV (dark circle) and 25 MeV (open circle) and $\theta_\gamma = 17.53°$.

case that $\theta_D \ll \chi_c$, and for those observation angles where the static contribution dominates, it turns out that the radiation yield depends on γ as $\ln \gamma$ and, therefore, this dependency is very weak for the projectile energy range under consideration. This fact is illustrated by Fig. 8, where we compare the radiation yields from the silicon crystal at electron-beam energy 25 MeV (averaged over 25 spectra) and 15 MeV. Note that for the same relations between χ_c and θ_D the energy dependency of the radiation yield for the atomic electron region will be $\gamma^2 \ln \gamma$.

V. CONCLUSION

Features of the incoherent cross section of x radiation produced by a relativistic electron in a crystal were studied for all momentum transfers. It was found that in the small-q region the fivefold incoherent cross section, considered as a function of the final electron angles, has sharp maxima and a minimum. To obtain the threefold cross section, the Monte-Carlo procedure was developed and relative contributions of different radiation mechanisms to this cross section have been analyzed. It is defined that at $\theta_\gamma > 10\gamma^{-1}$ crystal electrons give a dominant contribution to the total radiation yield. At such observation angles the radiation yield in crystals is essentially suppressed in comparison with the amorphous case.

The effect of suppression of incoherent x radiation from a silicon crystal, as well as a weak (logarithmic) dependence of incoherent intensity on the projectile energy, were demonstrated experimentally.

The obtained results show that experimental investigations of the features of incoherent x radiation in coincidence experiments are desirable. So far as the radiation generated at low momentum transfers is suppressed in crystals, investigations of properties of incoherent radiation in such kinds of experiments could make it possible to obtain more detailed information about the elementary processes of the electron nucleus and of electron-electron bremsstrahlung than it is possible with the use of amorphous targets. Moreover, the found properties of the radiation could be used in designing compact x-ray sources with optimal ratio of the coherent radiation component to incoherent bremsstrahlung.

ACKNOWLEDGMENTS

This work was partially supported by CNPq and FAPESP.

[1] J. Freudenberger *et al.*, Phys. Rev. Lett. **74**, 2487 (1994).
[2] D. I. Adejishvili *et al.*, Nucl. Instrum. Methods Phys. Res. B **152**, 406 (1999). It should be noted that in Eq. (1) of this reference the term in square brackets must be squared.
[3] D. I. Adejshvili *et al.*, Report No. KFTI 95-10, Kharkov, 1995 (unpublished).
[4] V. B. Gavrikov *et al.*, Braz. J. Phys. **29**, 516 (1999).
[5] S. V. Blazhevich *et al.*, Phys. Lett. A **195**, 210 (1994).
[6] V. B. Gavrikov *et al.*, Nucl. Instrum. Methods Phys. Res. A **457**, 411 (2001).
[7] M. L. Ter Mikaelyan, Zh. Eksp. Teor. Fiz. **25**, 296 (1953).
[8] H. Uberall, Phys. Rev. **103**, 1055 (1956).
[9] Derivation can be found in Appendix II of the book by M. L. Ter-Mikaelian, *High-Energy Electromagnetic Processes in Condensed Media* (Wiley-Interscience, New York, 1972).
[10] W. Heitler, *The Quantum Theory of Radiation* (Clarendon, Oxford, 1954).
[11] M. Ya. Amus 'ya, *et al.*, Sov. Phys. JETP **61**, 224 (1985).
[12] V. B. Gavrikov, Ph.D. thesis, Kharkov State University, Kharkov, 1996; available from the author upon request.
[13] J. H. Hubbell *et al.*, J. Phys. Chem. Ref. Data **4**, 471 (1975).
[14] A. I. Akhiezer and V. B. Beresetskii, *Quantum Electrodynamics* (Interscience, New York, 1965).
[15] M. N. Martins *et al.*, Nucl. Instrum. Methods Phys. Res. A **390**, 375 (1997).
[16] W. J. Cody and H. C. Thacher, Math. Comput. **23**, 289 (1969).
[17] D. I. Adejishivili *et al.*, Report No. KIPT 91-8, Kharkov, 1991, p. 14.
[18] Eq. (7.4d) in William T. Scott, Rev. Mod. Phys. **35**, 231 (1963).